Retrieval of Surface BRDF from Multiangle Remotely Sensed Data

Shunlin Liang[*,†] *and Alan H. Strahler*[*]

The bidirectional reflectance distribution function (BRDF) is the intrinsic measure of the directional properties of the Earth's surface. However, it cannot be measured directly by remote sensing. A procedure using the optimum technique is applied to retrieve surface BRDF parameters from multiangle remotely sensed data in which a statistical BRDF model and an analytical model of atmospheric radiative transfer are coupled. The atmospheric model decomposes radiant intensity received by a detector into four parts: scattered only by the (non-Lambertian) surface; singly scattered by the atmosphere; multiply scattered to the surface but unscattered to the detector; and multiply scattered before and after surface scattering. Analytical solutions are derived for the first two. The third is derived from a two-stream model, but incorporates the surface BRDF explicitly. The fourth uses a two-stream model under conditions of azimuthal independence. The six-parameter surface BRDF is modeled as the sum of a modified limacon function, which describes the basic bowl-shape of the BRDF, and a negative exponential, which describes the hotspot. Multiangle observations from the ASAS and PARABOLA instruments are analyzed using the coupled models. Experiments show that the simple statistical BRDF can summarize typical directional observations with errors in the range of 3–10%.

INTRODUCTION

As Gerstl has observed (1990), there are five generically different signature types in remote sensing: spectral signatures, temporal signatures, spatial signatures, angular signatures, and polarization signatures. Conventional research in remote sensing has concentrated on the use of spectral signatures based on nadir or near-nadir reflectance measurements. However, nadir reflectances are not always sufficient for remote sensing applications because many land surface covers have the same or nearly the same nadir spectral reflectance. This has led to exploration of the temporal and spatial domains, which have added significantly to our ability to infer land surface characteristics from remotely sensed data. Angular signatures are attractive because natural terrestrial surfaces reflect radiation quite anisotropically. The limitations of nadir reflectances in classification and other analyses have led to an exploration of the use of angular signatures.

Directional reflectance properties of earth surfaces were measured as early as the 1960s (Salomonson and Marlatt, 1968), and measurements have continued through the present (Ranson et al., 1984; Kimes et al., 1985; Deering, 1988; Jackson et al., 1990; Irons et al., 1991). In principle, the bidirectional reflectance distribution function (BRDF) fully describes the intrinsic directional reflectance of a surface. However, the BRDF cannot be directly measured by sensors for several reasons. First, the BRDF is defined as the ratio of two derivatives. Actual measurements will always involve finite intervals of solid angles defining the incident and viewing directions. Second, in the natural environment, the Earth's surface is always illuminated by sky radiance from the entire hemisphere, which does not satisfy the single-direction geometric condition of the BRDF. Finally, the path radiance and absorption of the atmosphere are always included in airborne or space-borne remotely sensed data. The important issue is to retrieve BRDF from multiangle observations, given these constraints. In this study, a procedure is developed for this purpose. There are two problems associated with BRDF retrieval if we assume that the solid angles of the sensors are very small: the correction of measurements for the path radiance of the atmosphere with the non-Lambertian surface as the lower boundary condition, and the deter-

[*]Center for Remote Sensing and Department of Geography, Boston University

[†]Present address: Department of Geography, University of Maryland, College Park, MD 20742.

Address correspondence to Alan Strahler, Center for Remote Sensing, Boston Univ., 725 Commonwealth Ave., Boston, MA 02215.

Received 1 November 1993; revised 27 April 1994.

0034-4257 / 94 / $7.00
©Elsevier Science Inc., 1994
655 Avenue of the Americas, New York, NY 10010

mination of the parameters that describe the shape of the BRDF.

Numerical algorithms have been widely used to evaluate the effects of non-Lambertian surfaces on atmospheric path radiance (Lee and Kaufman, 1986; Gerstl and Zardecki, 1985; Liang and Strahler, 1993a). However, these models are undesirable in the inversion experiments due to their need for extensive calculations. In order to retrieve surface structural information or directional reflectance, optimum algorithms are frequently employed, which involve hundreds or even thousands of such forward calculations. Fast algorithms are required for this purpose. For atmospheric radiative transfer, some analytical models exist, but most of these are used for radiative flux calculations, and are not directional. Typically, a Lambertian lower boundary condition is also assumed, which is unrealistic for real earth surfaces. Tanré et al. (1979) first developed an analytical formulation for a nonhomogenous non-Lambertian ground surface, which was recently used for the retrieval of Sahara dust optical thickness (Tanré and Legrand, 1991). However, their formulae are the corresponding versions of the Lambertian case based on similarity inference. No rigorous derivations have been given to support these formulae, although good experimental results have been reported (Tanre and Legrand, 1991). In this study, an alternative formulation is developed in which the radiation field is divided into four components, two of which are associated with a non-Lambertian lower boundary.

There are two approaches to analytical modeling of the BRDF—physical models and statistical models. Physical models relate the BRDF to various internal properties of the surface. For example, canopy reflectance models typically account for the directional reflectance of leaf canopies using leaf biophysical properties and the structural configuration of the canopy (Myneni et al., 1990; Goel, 1988). However, such physical models are oriented to specific objects (e.g., leaves). The general physical model for the BRDF of a mixture of many different objects has not been well formulated because it must accommodate a wide range of the environmental and physical conditions as well as viewing geometries.

Statistical models of the BRDF of a surface do not rely on physical parameters, but instead characterize the shape of the BRDF function using statistical parameters. Such characteristics provide a useful alternative to physical models, especially when we are faced with large number of directional observations and a complex surface. An early statistical characterization of a surface BRDF was provided for lunar surface reflectances by Minnaert (1941) using semiempirical photometric relationships with the reciprocity principle:

$$R(\theta_i,\theta) = r_0 \cos^{k-1}(\theta_i) \cos^{k-1}(\theta)\,, \tag{1}$$

where r_0 is the reflectance for overhead sun and nadir observation, θ_i and θ are the solar zenith angle and viewing angle, respectively, and k is a parameter describing the roughness state of the surface, varying typically between 0 and 1.0 for lunar surfaces. (Table 1 defines the major mathematical notation used in this text.) However, the dependence of reflectance on the azimuth angle is omitted in the above equation. Hapke (1963) and Veverka and Wasserman (1972) considered this dependence in some specific cases for theoretical studies. Further investigations of Minnaert's model are given by Kieffer et al. (1977) and Thorpe (1977). Pinty and Ramond (1986) apply this model to terrestrial surfaces taking into account single scattering of the Earth's atmosphere. Minnaert's model has a simple functional form, but does not seem accurate enough for complicated reflective surfaces.

Walthall et al. (1985) derived a three-parameter statistical model:

$$R(\theta_i,\varphi_i,\theta,\varphi) = a\theta^2 + b\theta \cos(\varphi - \varphi_i) + c\,, \tag{2}$$

where a, b, and c are parameters depending on incidence zenith angle (θ_i). This model has been widely used, but some important features observed within real datasets cannot be represented by the model (Walthall et al., 1985), notably some apparent furrow structures and the hotspot peak.

For desert and arid regions, Staylor and Suttles (1986) developed an analytic model as follows:

$$R(\theta_i,\theta,\varphi) = \frac{B(\mu,\mu_i)}{A(\mu_i)} \frac{1 + c_3(\mu\mu_i - \sin\theta_i \sin\theta \cos\varphi)^2}{1 + c_3[(\mu\mu_i)^2 + (1/2)(\sin\theta_i \sin\theta)^2]}\,, \tag{3}$$

where

$$B(\mu_i,\mu) = \frac{1}{\mu\mu_i}\left[c_1 + c_2\left(\frac{\mu\mu_i}{\mu + \mu_i}\right)^N\right],$$

$$A(\mu_i) = 2\int_0^1 B(\mu_i,\mu)\mu_i\, d\mu\,.$$

Here $\mu = \cos\theta$, c_1, c_2, c_3 and N are parameters to be estimated.

Another type of statistical directional reflectance model uses spherical harmonics (Goel and Reynolds, 1989), In this model, the directional reflectance function is expressed as a linear combination of spherical harmonics,

$$R(\theta,\varphi) = \sum_{m,n}[A_{mn} Y^e_{mn}(\theta,\varphi) + B_{mn} Y^o_{mn}(\theta,\varphi)]\,, \tag{4}$$

where $Y^e_{mn}(\theta,\varphi)$ and $Y^o_{mn}(\theta,\varphi)$ are even and odd harmonics, respectively. The parameters $A_{mn}(B_{mn})$ are evaluated based on the orthonormality of spherical harmonics. The most important feature of this model is that it can capture very fine structure in the directional reflectance function, if a sufficient number of terms of spherical harmonies are retained.

According to van de Hulst (1980), a desirable property of BRDF models is to satisfy the reciprocity princi-

Table 1. Notation

Symbol	*Description*
$A(\mu_i)$	plane albedo of the surface when the solar zenith angle is $\cos^{-1}(\mu_i)$
δ	Dirac delta function
$f(\Psi_A,\Psi_B)$	penalty function with atmospheric parameter set Ψ_A and BRDF parameter set Ψ_B
F_0	extraterrestrial solar irradiance
$F(\Psi_A,\Psi_B)$	merit function with atmospheric parameter set Ψ_A and BRDF parameter set Ψ_B
g	average asymmetric parameter of an aerosol/molecular atmosphere
g_a	asymmetric parameter of the aerosol
γ_i	parameters for two-stream approximation
h_s	height of the sensor in km
$H(\cdot)$	height correlation function for the optical depth calculations
$I^{us}(\tau,\Omega)$	unscattered solar radiance
$I^{ss}(\tau,\Omega)$	single-scattering radiance
$I^{ms\,1}(\tau,\Omega)$	first part of the multiple-scattering radiance
$I^{ms\,2}(\tau,\mu)$	second part of the multiple-scattering radiance
λ	wavelength
μ_0	cosine of the solar zenith angle (θ_0)
$\Omega(\mu,\varphi)$	unit vector of the solid angle with cosine of zenith angle μ and azimuth angle φ
$P(\Omega',\Omega)$	phase function of the atmosphere
φ_0	solar azimuth angle
ρ	spherical albedo of the surface
$R(\Omega',\Omega)$	BRDF of the surface
$r(\mu',\mu)$	azimuth-independent BRDF of the surface
τ	optical depth of a medium
τ_a	atmospheric optical depth ($\tau_{ae} + \tau_r$)
τ_{ae}	total aerosol optical depth
τ_r	total molecular optical depth
τ_{oz}	total ozone optical depth
τ_w	total water vapor optical depth
τ_{xs}	optical thickness above the sensor where x stands for a, ae, oz, w, r, etc.
ω	single-scattering albedo of aerosol

ple, in which reflectance is the same when viewing and illumination angles are interchanged. This constraint is also useful in deriving the solutions to a particular model formulation. While reciprocity is a property of atmospheric radiative transfer models and many surface scattering models, it is not necessarily required for canopy reflectance models. In the event that upper and lower leaf surfaces scatter light differently, then reciprocity will not necessarily be preserved. However, most physical models of leaf canopies assume bi-Lambertian leaf scattering, and thus obey the reciprocity principle. Since these models also fit leaf canopy BRDFs well, we may conclude that reciprocity is an acceptable assumption for the purposes of specifying a statistical BRDF model.

Beyond satisfying the reciprocity principle, a statistical BRDF model suited to remote sensing applications should have a simple, flexible function requiring only a few parameters, yet with a high ability to capture the details of the real BRDF. For this purpose, we propose a limaconlike model following Walthall et al. that is modified to accommodate a hotspot. It is discussed in the third section of this article.

There are two multiangle remote sensors involved in this study. The Advanced Solid-state Array Spectroradiometer (ASAS), is an airborne, off-nadir pointing, imaging spectroradiometer used to acquire bidirectional radiance data from terrestrial targets (Irons et al., 1991). The most interesting feature of this instrument is that it tilts up to 45° fore and aft in the direction of flight and is therefore capable of making directional images of a site on a single overpass with seven viewing angles. The Portable Apparatus for Rapid Acquisition of Bidirectional Observations of the Land and Atmosphere (PARABOLA) instrument (Deering and Leone, 1986) was designed to collect many multiangle measurements in order to analyze the BRDF of the earth surface and the sky. The PARABOLA is a battery-powered, three-channel (0.65–0.67 μm, 0.81–0.84 μm, 1.62–1.69 μm) radiometer that scans in a spherical pattern to acquire multiangle measurements.

An numerical optimization procedure is applied to retrieve the parameters of the proposed statistical BRDF model from ASAS, PARABOLA, and other directional observations through coupling with an atmospheric radiative transfer model. The inversion algorithm is described in the fourth section. The retrieved results from ASAS and PARABOLA are presented in the sixth and seventh sections. A brief discussion and conclusion is given in the last section.

AN ANALYTICAL MODEL OF ATMOSPHERIC RADIATIVE TRANSFER

For a plane-parallel, homogeneous atmosphere in the absence of clouds, the radiative transfer equation can be written as (Lenoble, 1985)

$$\mu\frac{\partial I(\tau,\Omega)}{\partial\tau} = I(\tau,\Omega) - \frac{\omega}{4\pi}\int_0^{4\pi} P(\Omega'\rightarrow\Omega)I(\tau,\Omega')\,d\Omega', \quad (5)$$

with the boundary conditions

$$\begin{cases} I(0,\Omega) = \delta(\Omega-\Omega_0)\pi F_0, & \mu<0, \\ I(\tau_0,\Omega) = \int_{2\pi} R(\Omega',\Omega)|\mu'|I(\tau_0,\Omega')d\Omega', & \mu>0, \end{cases} \quad (6)$$

where the solid angle Ω is characterized by the azimuth angle φ and the zenith angle θ with axis z or $\mu = \cos\theta$; μ is positive for upward radiation and negative for downward radiation; the azimuth angle φ is measured for an arbitrary original axis, generally clockwise when looking from bottom to top; ω is the single-scattering albedo; τ_0 is the total optical depth of the atmosphere; $P(\Psi)$ is the scattering phase function; $R(\Omega',\Omega)$ is the surface BRDF that will be discussed in the following section; $\delta(\Omega-\Omega_0)$ is the delta function; and F_0 is the extraterrestrial solar irradiance (Neckel and Labs, 1984). Note that a correction factor accounting for the seasonal variation of the Sun–Earth distance should also be used (Iqbal, 1983).

The scattering properties of the atmosphere depend on Rayleigh molecular and aerosol particles. We may further define the scattering phase function as the weighted average of Rayleigh and aerosol scattering phase function at the specific scattering angle:

$$P(\Psi) = \frac{p_r(\Psi)\tau_r + p_a(\Psi)\tau_{ae}}{\tau_r + \tau_{ae}},$$

subject to the constraint $1/2\int_0^{\pi} P(\Psi)\sin\Psi\,d\Psi = 1$. Here, τ_r and τ_{ae} are the molecular optical depth and aerosol optical depth of the whole atmosphere, respectively. The scattering phase angle, Ψ, is defined as

$$\cos(\Psi) = \mu\mu_0 + \sqrt{(1-\mu^2)(1-\mu_0^2)}\,\cos(\varphi-\varphi_0).$$

The molecular phase function is defined by the classical relation

$$p_r(\Psi) = 3/4(1+\cos^2\Psi),$$

and aerosol phase function takes the one-term Henyey–Greenstein (OTHG) function

$$p_a(\Psi) = \frac{(1-g_a^2)}{(1+g_a^2-2g_a\cos\Psi)^{1.5}},$$

where g_a defines the type of aerosol used in this evaluation of the scattering process.

If we observe the ground from the air using an instrument such as ASAS, we must consider the vertical distribution of scattering with the atmosphere. Assuming the height of the sensor is h_s above the ground, the molecular optical depth τ_{rs} can be obtained through the relation

$$\begin{cases} \tau_r = 0.0088\lambda^{-4.15+0.2\lambda}, & \lambda\ (\mu\text{m}), \\ \tau_{rs} = H_r(h_s)\tau_r, \end{cases}$$

with

$$H_r(h_s) = \exp(-0.1188h_s - 0.00116h_s^2),\ h_s\ (\text{km}),$$

as proposed by Van Stokkom and Guzzi (1984). For aerosol, the height correlation function is (Guzzi et al., 1987)

$$H_{ae}(h_s) = \exp(-h_s/H_p),$$

where H_p is the scale height, and is taken as 0.97 / 1.4 for the first 5 km above the earth surface (Penndorf, 1954). Then the aerosol optical depth at height h_s is $\tau_{aes} = H_{ae}(h_s)\tau_{ae}$.

The ozone optical depth can be obtained as

$$\begin{cases} \tau_{ox} = 0.03\exp[-277(\lambda-0.6)^2], & \lambda\ (\mu\text{m}), \\ \tau_{ozs} = \tau_{oz}H_{oz}(h_s), \end{cases}$$

with

$$H_{oz}(h_s) = \frac{1.0183}{1+0.0183\exp(h_s/5)}$$

as proposed by Lacis and Hansen (1974). The water vapor optical depth can be obtained by

$$\begin{cases} \tau_w = \dfrac{0.2385K_w(\lambda)C_w}{(1+20.07K_w(\lambda)C_w)^{0.45}}, \\ \tau_{ws} = H_w(h_s)\tau_w, \end{cases}$$

where $K_w(\lambda)$ (cm^{-1}) is the spectral absorption coefficient of water vapor (Leckner, 1978) and C_w (cm) is the precipitable water of the atmosphere. The height correlation function is due to Reitan (1963):

$$H_w(h_s) = \exp(-0.639h_s).$$

For convenience, let's define $\tau_a = \tau_r + \tau_{ae}$ and $\tau_s = \tau_{rs} + \tau_{aes}$ instead of using the total optical depth τ_0. From the above formulae, we can see that for a spaceborne sensor, $\tau_s = 0$, and for a ground radiometer, $\tau_s = \tau_a$, the total scattering optical depth.

It is well known that no analytical solution to Eq. (5) can be obtained. Although various numerical solutions are available, we need explicit solutions for inversion. The widely used two-stream approximations are quite simple and flexible. However, these are mainly used for radiative flux calculations and are reliable only for integrated quantities, as opposed to angular-dependent radiances. They usually assume a Lambertian surface as the bottom boundary.

To incorporate a non-Lambertian surface into the two-stream approximation and obtain more exact angular dependence of the upwelling radiance, we divide

the radiation field into four components: unscattered solar radiance, single-scattering radiance, and two multiple-scattering components. This decomposition is illustrated in Figure 1; (A) shows the unscattered solar (us) component and (B) the single-scattering (ss) component. The reason that the multiple-scattering radiance is divided into two parts is to incorporate the non-Lambertian reflectance of the boundary layer into the multiple-scattering calculations. The first part, shown in (C), is the downward-scattered radiance reflected by the non-Lambertian surface and received by the sensor without any further scattering by the atmosphere. The second part (D) is the rest of the multiple-scattering radiance. We will denote the first part of the multiple-scattering radiance as ms1, and the second part as ms2. In the following, the component ms2 will be assumed to be azimuth-independent.

Now let us describe the mathematical formulae for these components. For unscattered and single-scattered components, they are quite simple. When $\mu > 0$,

$$I^{us}(\tau,\Omega) = \pi F_0' |\mu_0| R(\Omega_0,\Omega) \exp\left(-\frac{\tau_a}{|\mu_0|} - \frac{\tau_a - \tau}{\mu}\right),$$

$$I^{ss}(\tau,\Omega) = \frac{\omega F_0' P(\Omega_0,\Omega)|\mu_0|}{4(|\mu_0| + \mu)} \times \left\{\exp\left(\frac{\tau}{|\mu_0|}\right) - \exp\left[\frac{\tau}{\mu} - \tau_a\left(\frac{1}{|\mu_0|} + \frac{1}{\mu}\right)\right]\right\}. \quad (7)$$

When $\mu < 0$,

$$I^{us}(\tau,\Omega) = \pi F_0' \delta(\Omega - \Omega_0) \exp\left(-\frac{\tau}{|\mu_0|}\right),$$

$$I^{ss}(\tau,\Omega) = \frac{|\mu_0| F_0' \omega P(\Omega_0,\Omega)}{4(|\mu_0| - |\mu|)}\left[\exp\left(-\frac{\tau}{|\mu_0|}\right) - \exp\left(-\frac{\tau}{|\mu|}\right)\right], \quad \mu \neq \mu_0$$

$$I^{ss}(\tau,\Omega) = \frac{\omega F_0' \tau}{4|\mu_0|} P(\Omega_0,\Omega) \exp\left(-\frac{\tau}{|\mu_0|}\right), \quad \mu = \mu_0. \quad (8)$$

where F_0' is the extraterrestrial irradiance attenuated by ozone and water vapor:

$$F_0' = F_0 \exp\left(-\frac{\tau_{oz} + \tau_w}{|\mu_0|} - \frac{\tau_{oz} - \tau_{ozs} + \tau_w - \tau_{ws}}{\mu}\right).$$

The formulae for the multiple-scattering components cannot be derived explicitly, so we will use the two-stream approximation in our formulation. If we decompose the unscattered radiance from Eq. (5), the corresponding equation for the scattered radiance will have one more source term contributed by the unscattered radiance. By defining the new quantity

$$I(\tau,\mu) = \int_0^{2\pi} I(\tau,\mu,\varphi)\, d\varphi,$$

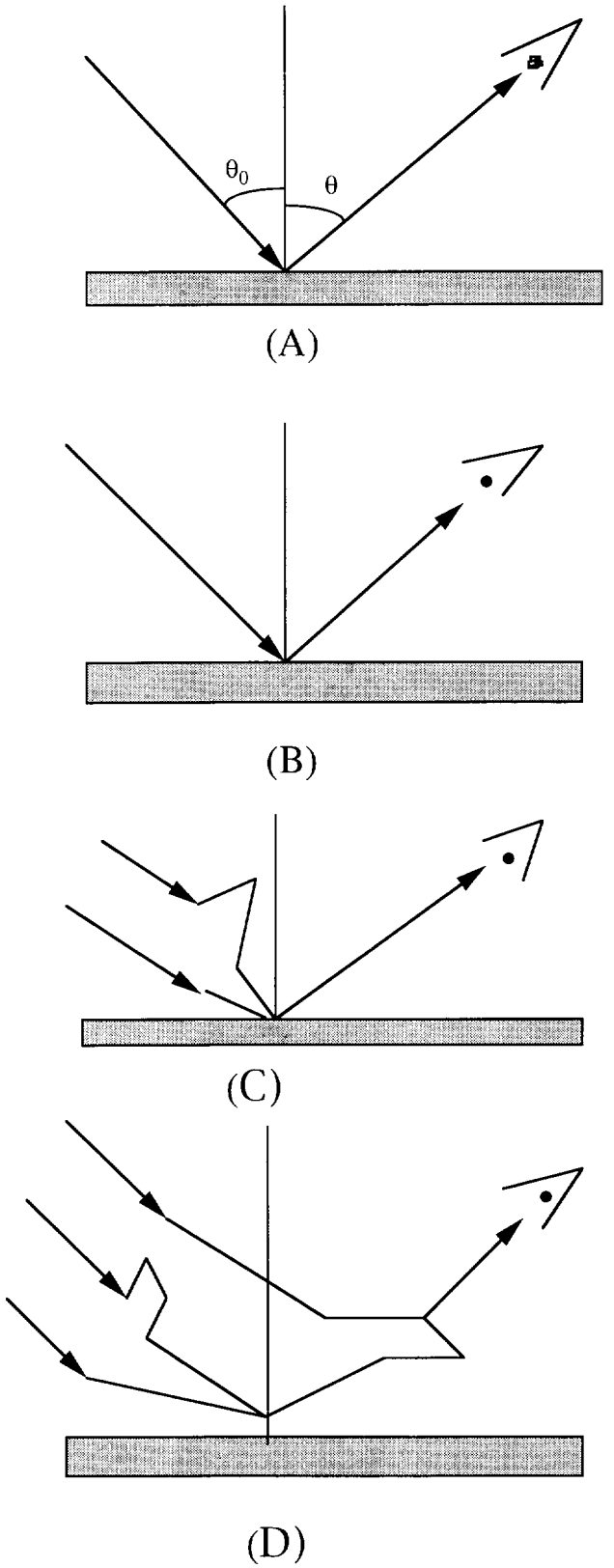

Figure 1. Illustration of the radiation field decomposition.

integration over the azimuth angle yields the azimuth-independent radiative transfer equation (Meador and Weaver, 1980)

$$2\mu\frac{dI(\tau,\mu)}{d\tau} = 2I(\tau,\mu) - \omega\int_{-1}^{1} p(\mu,\mu')I(\tau,\mu')\,d\mu' - \omega\pi F_0' p(\mu,\mu_0) \times \exp(-\tau/|\mu_0|), \tag{9}$$

subject to the boundary conditions

$$I(0,\mu) = 0, \quad \mu < 0,$$

$$I(\tau_a,\mu) = \int_{-1}^{0} I(\tau_a,\mu')r(\mu',\mu)|\mu'|d\mu' + \pi F_0'|\mu_0|\exp\left(\frac{-\tau_a}{|\mu_0|}\right) \times r(\mu_0,\mu), \quad \mu > 0. \tag{10}$$

Here, $p(\mu,\mu')$ and $r(\mu',\mu)$ are the azimuth-independent phase function and surface BRDF, defined as

$$p(\mu,\mu') = \frac{1}{2\pi}\int_0^{2\pi} P(\mu,\varphi,\mu',\varphi')\,d\varphi' = \sum_{l=0}^{\infty}(2l+1)g_l P_l(\mu)P_l(\mu'),$$

$$r(\mu,\mu') = \frac{1}{2\pi}\int_0^{2\pi} R(\mu',\mu,\varphi)\,d\varphi,$$

where $g_l = 1/2\int_{-1}^{1} P_l(\mu)p(\mu,1)\,d\mu$ and $P_l(\mu)$ is the Legendre polynomial function of order l. In the following two-stream approximation, only the first two terms are considered for the phase function $p(\mu,\mu')$.

There are many versions of the two-stream approximation. Meador and Weaver (1980) have shown that a whole class of approximate two-stream solutions can be reduced to a standard form with only a few coefficients. The required hemispherical integrals

$$I^+(\tau) = \int_0^1 \mu I(\tau,\mu)\,d\mu,$$

$$I^-(\tau) = \int_{-1}^{0} |\mu| I(\tau,\mu)\,d\mu \tag{11}$$

can be obtained by solving a coupled ordinary differential equation set. Meador and Weaver put forward a hybrid Eddington-delta algorithm for this, which has proven to be generally superior to the classic two-stream approximations over a wide range of atmospheric conditions. For $I^{\pm}(\tau)$, Meador and Weaver present formulae for a black surface. We earlier extended this to a Lambertian surface with arbitrary reflectance ρ (Liang and Strahler, 1993b). In that article, no absorbing gases are considered: For convenience, these formulae are shown in the appendix with the corresponding modifications. After obtaining the $I^{\pm}(\tau)$, the radiance formulae from the hybrid Eddington-delta algorithm are (Meador and Weaver, 1980):

$$\hat{I}(\tau,\mu) = \frac{(1-g^2)u + g^2\delta(\mu+\mu_0)I^+(\tau)}{1-g^2(1-|\mu_0|)}, \quad \mu > 0,$$

$$\hat{I}(\tau,\mu) = \frac{(1-g^2)u + g^2\delta(\mu-\mu_0)I^-(\tau)}{1-g^2(1-|\mu_0|)}, \quad \mu < 0, \tag{12}$$

where $g = \tau_{ae}g_a / (\tau_{ae} + \tau_r)$, and u is defined as

$$u = (1 + 1.5\mu)I^+(\tau) + (1 - 1.5\mu)I^-(\tau).$$

Unfortunately, these radiance formulae are not realistic enough in terms of the angular dependence when $\mu > 0$. For example, the dependence of upwelling radiance on μ is linear, so that when the viewing angle is larger (μ is smaller), the upwelling radiance becomes smaller. It is obvious that this is not the correct angular dependence. Instead, we will derive more accurate radiance formulae based on (9). Since the terms $I^{\pm}(\tau)$ have been explicitly calculated, we will use them to approximate the integration term in (9) so that (9) becomes an ordinary differential equation. A similar approach was used by Kaufman (1979).

Using the approximate relation $p(\mu,\mu') = \omega(1 - 3g\mu\mu')$ for the part of the Eddington approximation, it is not difficult to get the approximate form of (9):

$$2\mu\frac{d\hat{I}(\tau,\mu)}{d\tau} = 2\hat{I}(\tau,\mu) - aI^+(\tau) - bI^-(\tau) - \omega\pi F_0' p(\mu,-|\mu_0|) \times \exp\left(-\frac{\tau}{|\mu_0|}\right), \tag{13}$$

where a and b are given by

$$a = \frac{\omega(1-g^2)(4+3g\mu) + 2\omega g^2 p(\mu,|\mu_0|)}{2[1-g^2(1-|\mu_0|)]},$$

$$b = \frac{\omega(1-g^2)(4-3g\mu) + 2\omega g^2 p(\mu,-|\mu_0|)}{2[1-g^2(1-g^2(1-|\mu_0|)]}. \tag{14}$$

Solving Eq. (13) for $\mu < 0$, we get

$$\hat{I}(\tau,\mu) = D_1\ \exp(\eta\tau) + D_2 \times \exp(-\eta\tau) + D_3\ \exp(\tau/\mu_0) + E_1\ \exp(\tau/\mu), \tag{15}$$

where the coefficients are given by

$$D_1 = \frac{a\gamma_2 + b(\gamma_1 - \eta)}{2\gamma_2(1-\eta\mu)}X_1,$$

$$D_2 = \frac{a\gamma_2 + b(\gamma_1 + \eta)}{2\gamma_2(1+\eta\mu)}X_2,$$

$$D_3 = \frac{|\mu_0|[a\gamma_2 X_3 + bt_0 + \pi\omega F_0' p(\mu,\mu_0)\gamma_2]}{2\gamma_2(|\mu_0| + \mu)}$$

for $\mu \neq \mu_0$. If $\mu = \mu_0$, then D_3 is

$$D_3 = \frac{[aX_3\gamma_2 + bt_0 + \pi\omega F_0' p(\mu,\mu_0)\gamma_2]\tau}{2|\mu|\gamma_2}.$$

Parameters X_i ($i=1, 2, 3$), η, t_0, and γ_i ($i=1, 2, 3$) are given in the Appendix. From the boundary condition $I(0,\mu)=0$, E_1 can be determined as

$$E_1 = \begin{cases} -(D_1+D_2+D_3), & \mu \neq \mu_0, \\ -(D_1+D_2), & \mu = \mu_0. \end{cases}$$

For $\mu > 0$, we obtain the similar solution

$$\hat{I}(\tau,\mu) = D_1 \exp(\eta\tau) + D_2 \exp(-\eta\tau) + D_3 \exp(-\tau/|\mu_0|) + E_1' \exp(\tau/\mu), \quad (16)$$

where parameters D_1, D_2, and D_3 are the same as above. From the lower boundary condition, the constant E_1' can be determined as

$$E_1' = \exp(-\tau_a/\mu)[I(\tau_a,\mu) - D_1 \exp(\eta\tau_a),$$

where $I(\tau_a,\mu)$ is given in (10). Since $I(\tau,\mu)$ is defined as an integrated quantity over the azimuth direction in (8), the average radiance in a single direction must be divided by 2π.

To summarize, the radiation field has been divided into four parts. The unscattered radiance $I^{us}(\tau,\Omega)$ and single-scattering radiance $I^{ss}(\tau,\Omega)$ are expressed in (7) and (8). To derive $I^{ms\,1}(\tau,\Omega)$ and $I^{ms\,2}(\tau,\Omega)$, an azimuth-independent radiative transfer equation is used and its solutions are derived with an aid of integrated radiances. Notice that the solutions (15) and (16) to the azimuth-independent radiative transfer equation include all orders of scattering. The single-scattering counterpart of the radiances $I^{ss}(\tau,\mu)$ have the same formulae as (15) and (16) except that γ_1 and γ_2 [(A4)] will be replaced by γ_1' and γ_2' [(A6)] and ρ is set to zero.

Now let us go back to the multiple-scattering calculation. The component ms 1 can be expressed as

$$I^{ms\,1}(\tau,\Omega) = \exp\left(-\frac{\tau_a-\tau}{\mu}\right)\int_0^1\int_0^{2\pi} I^d(\tau_a,\Omega')R(\Omega',\Omega)|\mu'|\, d\Omega', \quad (17)$$

where $I^d(\tau_a,\Omega')$ is the total downward sky radiance, which is the sum of the exact single-scattering component (8) and the approximate multiple-scattering component, or

$$I^d(\tau_a,\Omega) = I^{ss}(\tau_a,\Omega) + \hat{I}(\tau_a,\mu)/2\pi - \hat{I}^{ss}(\tau_a,\mu). \quad (18)$$

To obtain $I^{ms\,2}(\tau_s,\mu)$, we need to know the corresponding azimuth-integrated ms 1 component, which will be denoted by $\hat{I}^{ms\,1}(\tau,\mu)$ and the single-scattering component $I^{ss}(\tau,\mu)$. For only the upwelling radiance, $\hat{I}^{ms\,1}(\tau,\mu)$ can be computed by

$$\hat{I}^{ms\,1}(\tau,\mu) = 2\pi \exp\left(-\frac{\tau_a-\tau}{\mu}\right)\int_0^1 \hat{I}^d(\tau_a,\mu')r(\mu',\mu)|\mu'|\, d\mu', \quad (19)$$

where $I^d(\tau_a,\mu')$ is the azimuth-independent counterpart of the downward sky radiance (18). Thus, the component ms 2 can be calculated by

$$I^{ms\,2}(\tau,\mu) = \hat{I}(\tau,\mu)/2\pi - \hat{I}^{ms\,1}(\tau,\mu) - I^{ss}(\tau,\mu). \quad (20)$$

The total upwelling radiance arriving at the sensor is then the sum of these four components:

$$I(\tau_s,\Omega) = I^{us}(\tau_s,\Omega) + I^{ss}(\tau_s,\Omega) + I^{ms\,1}(\tau_s,\Omega) + I^{ms\,2}(\tau_s,\mu). \quad (21)$$

From the above formulae, we can see that $I^{us}(\tau,\Omega)$ and $I^{ss}(\tau,\Omega)$ are exactly derived, $I^{us}(\tau,\Omega)$ and $I^{ms\,1}(\tau,\Omega)$ employ the exact BRDF of the surface, and $I^{ms\,2}(\tau,\mu)$ is calculated based on an azimuth-averaged BRDF.

A STATISTICAL BRDF MODEL

In this section, a statistical BRDF model will be discussed to describe the directional reflectance of the Earth surface. Existing directional reflectance models have been briefly summarized in the introduction. For applications with such existing sensors as ASAS or planned sensors such as MISR (Multiangle Imaging Spectroradiometer) (Diner et al., 1989), which have only a limited number of viewing directions, the total parameters in the statistical BRDF model will need to be smaller than 7 (for ASAS in the principal plane) or 9 (for MISR). On the other hand, the use of too few parameters may lead to a loss of some important information in the BRDF. Our approach is to separate the BRDF into two additive components—a bowl-shaped component and a hotspot component. The limacon function (Walthall et al., 1985) is modified to model the bowl-shaped component, and the hotspot component is modeled by an exponential function. The model can be expressed as

$$R(\Omega_i,\Omega) = f_1(\Omega_i,\Omega) + f_2(\Omega_i,\Omega), \quad (22)$$

where f_1 is the bowl-shaped component and f_2 is the hotspot component:

$$\begin{cases} f_1(\Omega_i,\Omega) = b_0 + b_1\theta_i\theta\cos(\varphi-\varphi_i) + b_2\theta_i^2\theta^2 + b_3(\theta_i^2+\theta^2), \\ f_2(\Omega_i,\Omega) = a_0\exp[-a_1\tan(\pi-\alpha)], \end{cases}$$

where α is the phase angle between the incident direction and the viewing direction. If the viewing direction coincides with the solar incidence direction, then $\alpha=\pi$, and f_2 approaches the maximum. It is obvious that this model satisfies the reciprocity principle.

We note that this BRDF formulation easily lends itself to retrieval of hemispheric surface reflectance using multiangle observations, which should be considered more accurate than estimation from nadir or single-angle viewing (Kimes et al., 1987; Starks et al., 1991; Kimes and Deering, 1992). Our present procedure can be used to retrieve not only the plane albedo, but also possibly the spherical albedo from a set of directional radiance data obtained in the presence of sky radiance. The plane albedo using our present model can be calculated by

$$A(\mu_i) = \int_{2\pi^+} [f_1(\Omega_i,\Omega) + f_2(\Omega_i,\Omega)]\mu\, d\Omega, \quad (23)$$

where $2\pi^+$ represents the upper hemisphere. The spherical albedo ρ is given by

$$\rho = 2\int_{-1}^{0} A(\mu')|\mu'|\, d\mu'. \quad (24)$$

INVERSION ALGORITHM DESCRIPTION

For remote sensing applications, we often wish to extract surface BRDF from remote sensed directional radiance data. We propose here an optimum technique to invert BRDF parameters through minimizing a merit function consisting of a sum of squares of the residual (SSR) and a penalty function:

$$F(\Psi_A,\Psi_B) = \sum_{k=1}^{K} w_k[I_k - \hat{I}_k(\Psi_A,\Psi_B)]^2 + f(\Psi_A,\Psi_B), \qquad (25)$$

where w_k is the weight factor, I_k is the measured radiance, $I_k(\Psi_A,\Psi_B)$ is the predicted radiance by models with canopy BRDF parameters Ψ_A and atmosphere parameters Ψ_B, and $f(\Psi_A,\Psi_B)$ is the penalty function, which keeps estimated parameters or their functions in reasonable regions. In all of the following calculations, $w_k = 1$ ($k = 1,2,\ldots,K$) have been assumed.

The construction of the penalty function is simple. Based on constraint functions, say, $g_i(\Psi_A,\Psi_B) > 0$, the Siddall algorithm (Siddall, 1972) is

$$f(\Psi_A,\Psi_B) = 10^{20}\sum_{\hat{I}} |g_i(\Psi_A,\Psi_B)|, \qquad (26)$$

where $\hat{I}$ identifies the set of violated constraints, that is,

$$g_i(\Psi_A,\Psi_B) < 0,$$

for all i in $\hat{I}$. The constraint function comes from a series of constraints on either individual parameters or their functions. For example, the single-scattering albedo ω should be $0 \leqslant \omega \leqslant 1$; the spherical albedo ρ should be $0 < \rho < 1$. In this study, we assume that the atmosphere parameters Ψ_B are known; thus only BRDF parameters are to be estimated.

In order to find optimal estimates of these parameters, an iteration process is necessary. At each iteration, the iteration length and iteration direction needs to be determined. To date, the most successful direct search algorithm is the method due to Powell (1964), especially with the modifications suggested by Zhangwill (1967) and Brent (1973), which we will refer to as the Powell algorithm. One of the better features of this algorithm is that we do not need to derive the derivatives of the merit function, which is frequently very difficult. Thus, we can incorporate any kind of penalty function to get realistic solutions. This algorithm has been recently used for the inversion of canopy radiative transfer models (Kuusk, 1991; Liang and Strahler, 1993b).

MODEL VALIDATION

Our analytical model of the atmospheric radiative transfer was validated by comparison with the numerical model of Liang and Strahler (1993a) for different aerosol optical depths. This model solves the atmospheric radiative transfer equation for directional radiance over a non-Lambertian surface using the Gauss–Seidel iteration algorithm. The upwelling radiance is normalized as reflectance $I(0,\Omega)\pi / (\mu_0 F_0)$. The parameters selected for radiation calculations are: $\theta_0 = 30°$, $\varphi_0 = 0°$, $F_0 = 1.0$ mW cm^{-2}, $g_a = 0.65$, $\omega = 0.94$. To provide the parameters of the non-Lambertian background BRDF, we fitted our statistical BRDF model to dense soybean data measured by Ranson et al. (1984) in Band 1 (green) and Band 4 (near-infrared) as discussed further below. For the validation exercise, we normalized these BRDFs to hemispherical albedos of 0.1 and 0.3 in the two bands, respectively. The BRDF parameters are shown in Table 2. We also calculated reflectance with the analytical model for a Lambertian surface with the same albedo in order to contrast the difference between Lambertian and non-Lambertian boundary conditions.

Figure 2 compares δ-two-stream solutions for the aerosol atmosphere over the non-Lambertian surface and its equivalent Lambertian surface with "exact" Gauss–Seidel solutions at three different optical depths. When $\tau = 0.05$ (A), most reflected radiance at the top of the atmosphere is from the ground reflectance. Thus, the equivalent Lambertian surface reflects radiance in different viewing angles nearly isotropically, and fits the Gauss–Seidel reflectance poorly. When $\tau = 0.25$ (C), the atmosphere is quite turbid. In this case, the path radiance of the atmosphere constitutes a large proportion of the total upwelling radiance, so that the difference between the calculated reflectance for the non-Lambertian surface and the equivalent Lambertian surface becomes smaller. Regarding the performance of the non-Lambertian parametric model, we can see that the δ-two-stream approximation based on the real non-Lambertian surface can yield very good angular patterns for this range of the optical depth, although the calculated reflectances are systematically smaller than the Gauss–Seidel solutions (the relative error is about 5–15%). Thus, incorporating a non-Lambertian BRDF into the δ-two-stream formulation can significantly improve its accuracy. However, the validation shows that, as the optical depth in-

Table 2. Parameters for the Statistical BRDF

	Parameters					
Albedo	b_0	b_1	b_2	b_3	a_0	a_1
0.10	−0.37532	0.00895	0.00275	0.01240	0.40356	0.03900
0.30	0.01277	0.00543	0.00064	0.02011	0.08012	0.41800

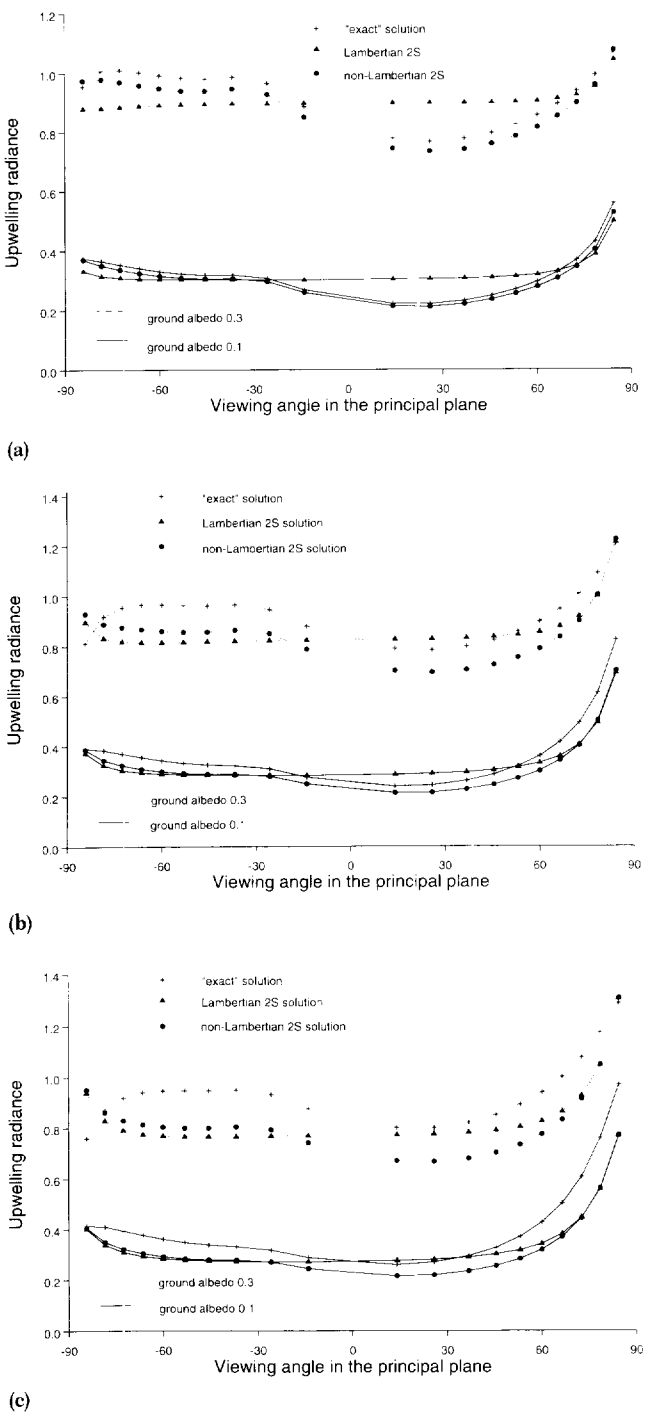

Figure 2. Validation of the δ-two-stream algorithm using Gauss-Seidel algorithm for the aerosol atmosphere. The solar zenith angle is 30°, and the solar azimuth angle is 0°. The aerosol optical depth in A–C is 0.05, 0.15, and 0.25.

creases, the relative error between the analytical model and the more accurate iterative solution becomes larger. Thus, there is still a need for more accurate analytical methods. A δ-four-stream approximation incorporating a non-Lambertian surface has been developed (Liang and Strahler, 1994), which could easily be substituted into the present formulation.

To evaluate the applicability of the statistical BRDF model, the soybean reflectance data measured by Ranson et al. (1984) were used to test this model. The soybean data are not BRDF measurements, but rather bidirectional reflectance functions (BRFs), which include sky radiance. However, under clear sky conditions at longer wavelengths, the BRF divided by π approaches the BRDF if the field of view of the sensor is small. Accordingly, we selected datasets from twelve sun positions on a clear day with low sky radiance from the data from Ranson et al. (1984). The viewing zenith angles consist of 0°, 7°, 15°, 22°, 30°, 45°, and 60° and the viewing azimuth angles are 0°, 45°, 90°, 135°, 180°, 225°, 270°, and 315°. A further description of these data can be found in their technical report (Ranson et al., 1984).

To assess the goodness of fit, we examine the relative error, defined as

$$\frac{1}{N}\sum_{i=1}^{N}\frac{|r_i-\hat{r}_i|}{r_i}, \tag{27}$$

where r_i and $\hat{r}_i$ are the measured and fitted reflectance, respectively, and N is the total number of data values; here, $N=575$. The relative errors for Band 4 (near-infrared, Table 3) are illustrated in Figure 3, where the sign of the difference has been retained. It seems that the errors for the first two sets of reflectance (about first 90 observations) are a little larger than the others. The relative errors for the other sets of reflectance appear quite randomly distributed. Table 3 provides the values for the fitted parameters and mean relative errors for all four bands. Note that no hotspot component is fitted for Band 3 ($a_1=0$). When examining the raw data, we found that the reflectance near the hotspot region is not obviously larger in this band. If a relative error of 2–4% is acceptable in the fitting experiment, it implies that six parameters can effectively summarize 575 directional reflectance measurements as a single, coherent BRDF function.

ASAS DATA BRDF EXTRACTION

In another exercise, we applied the BRDF model to directional reflectances observed with the Advanced Solid-state Array Spectroradiometer (ASAS). To retrieve BRDF from the ASAS data, we selected five sites along a conifer forest transect of Oregon (the OTTER transect; Peterson and Waring, 1994). The principal plane ASAS radiances and independently-modeled geometric-optical BRDFs in ASAS Band 25 (near-infrared, 788–805 nm) are compared in the Abuelgasim and Strahler (1994).

Since several sites in the OTTER database also have imagery in the cross-principal plane, which is perpendicular to the principal plane, an experiment was carried

Table 3. Inversion Results for the Soybean Data

	Inverted Parameters						
Wavelength (nm)	b_0	b_1	b_2	b_3	a_0	a_1	*Relative Error (%)*
500–600	−0.1735	0.0041	0.0013	0.0057	0.1865	0.039	2.70
600–700	−0.1751	0.0038	0.0013	0.0048	0.1868	0.035	4.09
700–800	−0.0885	−0.0216	0.0277	−0.0070	0.1910	0.0000	5.08
800–1100	0.0216	0.0092	0.0010	0.0344	0.1362	0.418	2.70

out to evaluate the effects of the different number of images on the BRDF inversion. The inversion programs were run twice for each site, one with the input of the datasets only in the principal plane (seven viewing angles), another with all 13 viewing angles. The results for two of the sites are illustrated in Table 4, in which the plane albedo $A(\theta_0)$ is also given. N stands for the number of the viewing angles in the input datasets. The relative error measures the fit of the BRDF model to the ASAS radiance data. Notice that when we use (27) to calculate the relative error, r_i and $\hat{r}_i$ would refer to radiances instead of reflectances. Since both imagery in the principal plane and cross-principal plane were acquired at different times in the same day (about 20 min delay), the datasets were normalized so that the radiance in the nadir direction is the same.

The calculations show that the relative differences of the retrieved reflectances in the principal plane are less than 1%, but increases when both principal and cross-principal data are fitted. The retrieved albedoes have larger differences. It seems reasonable that albedoes retrieved with all 13 viewing angles tend to be a little smaller because principal plane values likely include some bright values, such as the hotspot or a strong forward scattering peak in some cases.

PARABOLA DATA BRDF EXTRACTION

The Portable Apparatus for Rapid Acquisition of Bidirectional Observations of the Land and Atmosphere (PARABOLA) instrument has a much larger number of viewing angles than ASAS and path radiances are inconsequential (Deering and Leone, 1986). In this experiment, we arbitrarily selected a few shinnery oak reflectance datasets measured in 1984 in Texas (kindly provided by Dr. Deering). Each dataset is for one site with a specific solar incidence direction. The retrieved parameters are listed in Table 5. Here, only the first two visible and near-infrared bands (0.65–0.67 μm and 0.81–0.84 μm) are considered. The same procedure can be applied to process other bands. Constant atmospheric parameters for all sites have been assumed for simplicity: $F_0 = 154.77\ E_0$, $\tau_{ae} = 0.055$ for the first band, and $F_0 = 107.76\ E_0$, $\tau_{ae} = 0.023$ for the second band, where E_0 is the correction factor for the variation of the Earth–Sun distance as provided by Iqbal (1983), $\omega_0 = 0.94$ and $g = 0.65$. The relative errors are a little larger than those of the other datasets examined, but the results are quite satisfactory.

Figure 3. Relative errors of fitted soybean reflectances (800–1100 nm).

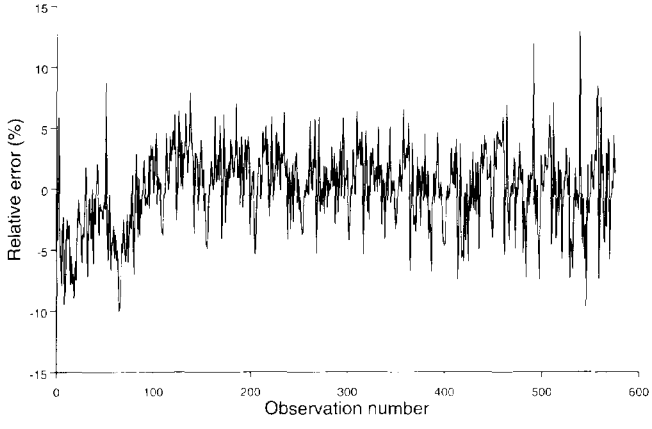

DISCUSSION AND CONCLUSIONS

A procedure to retrieve BRDF from multiangle remotely sensed data has been discussed above in which a statistical BRDF model and an analytical model of atmospheric radiative transfer are developed. The six-parameter statistical BRDF model contains six parameters, and thus seems quite suitable for such directional data as ASAS and MISR, which have a limited number of observation directions. Experiments show that the statistical BRDF model can summarize soybean data measured by Ranson et al. (1984) at 12 solar incident conditions with a relative error of about 3–5% for four different bands. Although PARABOLA has a much larger number of observing directions, the proposed model cannot capture more details in the BRDF. Therefore, a model with a flexible parameter set would be desired for various types of directional data.

With a new decomposition of the radiation field, the non-Lambertian lower boundary condition is incorporated into a two-stream approximation for the multiple-scattering calculation so that more realistic upwelling radiance distribution and downward sky radiance distribution are obtained. This model fits "exact" calculations quite well when the optical depth is small. In the visible region, atmospheric effects are much larger than in the near-IR region, and here a better parameterization scheme for multiple scattering may be desirable, especially

Table 4. Inversion Results from the ASAS Data

Site Name	θ_0°	Inverted Parameters $A(\theta_0)$	b_0	b_1	b_2	b_3	a_0	a_1	Relative Error (%)
Juniper	50.3	0.3204	0.0281	−0.0576	0.0026	0.0130	0.0656	0.2014	2.64
Scio	52.5	0.6698	0.1700	−0.0826	0.0641	−0.0176	0.3685	3.2896	1.08
Cascade Head	22.3	0.3418	0.1099	−0.0639	−0.5881	0.1075	0.1361	1.2967	1.11
Waring Woods	22.4	0.3500	−0.0815	0.0773	−3.2581	0.5250	0.4028	1.0825	3.17
Metolius	47.5	0.6244	0.1485	−0.1049	0.0927	−0.0026	0.0706	4.3322	0.49

Table 5. Inversion Results for the PARABOLA Data

Data set	θ_0°	Band Number	Inverted Parameters b_0	b_1	b_2	b_3	a_0	a_1	Relative Error (%)
tex84g43.aff	30.9	2	0.1671	−0.0012	0.3811	0.0125	0.5206	0.8483	5.64
tex84g43.aff	30.9	1	0.0830	−0.0253	−0.0658	0.0434	0.2254	1.6173	8.04
tex84h16.aff	46.9	2	0.3097	−0.0722	0.4379	−0.1303	0.5885	1.0832	5.02
tex84h16.aff	46.9	1	0.0194	−0.0054	0.0477	0.0076	0.2865	0.9298	6.15
tex84h34.aff	61.9	2	0.3540	−0.0805	0.2396	−0.0534	0.6366	1.5649	6.69
tex84h34.aff	61.9	1	0.0608	−0.0289	0.0401	0.0189	0.2603	1.7825	7.00
tex84i02.aff	70.7	2	0.3595	−0.1074	0.2001	−0.0313	0.6366	2.3524	8.65
tex84i02.aff	70.7	1	0.0573	−0.0379	0.0521	0.0159	0.3595	2.8939	9.26

for turbid atmospheres. Our four-stream model (Liang and Strahler, 1993c) would be an appropriate candidate.

Surface hemispherical reflectance (plane albedo) should be estimated more accurately from multiangle remotely sensed observations than from the nadir or any other single direction. Existing approaches using so-called "strings" of directional data typically calculate the albedo by deriving an approximate integration based on the limited observation directions. An obviously different approach to the calculation of the plane albedo is reported in this article. According to our schema, the reflectances at other viewing directions are interpolated using the statistical BRDF model, so that an exact numerical integration formula can be applied to calculate the plane albedo. More research is required to evaluate the accuracy of the albedo calculation using this scheme and to test its sensitivity to various factors.

APPENDIX: INTEGRATED UPWARD AND DOWNWARD RADIANCES

These formulae have been discussed in our previous article (Liang and Strahler, 1993b). $I^{\pm}(\tau)$ are given by

$$I^+(\tau) = X_1 \exp(\eta\tau) + X_2 \exp(-\eta\tau) + X_3 \exp(-\tau/|\mu_0|),$$
$$I^-(\tau) = (1/\gamma_2)[(\gamma_1 - \eta)X_1 \exp(\eta\tau) + (\gamma_1 + \eta)X_2 \times \exp(-\eta\tau) + t_0 \exp(-\tau/|\mu_0|)], \quad \text{(A1)}$$

where X_i ($i = 1, 2, 3$) are defined as

$$X_1 = \frac{t_0 w_2 - w_0(\gamma_1 + \eta)}{(\eta + \gamma_1)w_1 + (\eta - \gamma_1)w_2},$$
$$X_2 = -\frac{t_0 w_1 - w_0(\gamma_1 - \eta)}{(\eta + \gamma_1)w_1 + (\eta - \gamma_1)w_2},$$
$$X_3 = \frac{\pi F_0' \omega(\gamma_1\gamma_3 + \gamma_2\gamma_4 - \gamma_3/|\mu_0|)}{\eta^2 - 1/\mu^2}. \quad \text{(A2)}$$

Other parameters are given by

$$t_0 = (\gamma_1 + 1/|\mu_0|)X_3 - \pi F_0'\omega\gamma_3,$$
$$w_0 = \{[\rho(\gamma_1 + 1/|\mu_0|) - \gamma_2]X_3 + \pi F_0'\rho(|\mu_0| - \omega\gamma_3)\} \times \exp(-\tau_a/|\mu_0|),$$
$$w_1 = [\rho(\gamma_1 - \eta) - \gamma_2]\exp(\eta\tau_a),$$
$$w_2 = [\rho(\gamma_1 + \eta) - \gamma_2]\exp(-\eta\tau_a),$$
$$\eta = \sqrt{\gamma_1^2 - \gamma_2^2}. \quad \text{(A3)}$$

The parameters characterizing the hybrid Eddington-delta algorithm are

$$\gamma_1 = \frac{7 - 3g^2 - \omega(4 + 3g) + \omega g^2(4\beta + 3g)}{4[1 - g^2(1 + \mu_0)]},$$
$$\gamma_2 = \frac{g^2 - 1 + \omega(4 - 3g) + \omega g^2(4\beta + 3g - 4)}{4[1 - g^2(1 + \mu_0)]},$$
$$\gamma_3 = \beta, \quad \text{(A4)}$$

where β is the backscatter fraction, defined as

$$\beta = 1/2\int_0^1 p(|\mu_0|, -\mu')\,d\mu'. \quad \text{(A5)}$$

For the approximate single-scattering component, γ_1 and γ_2 must be replaced by γ_1' and γ_2' defined as

$$\gamma_1' = \frac{7 - 3g^2}{4[1 - g^2(1 - |\mu_0|)]},$$
$$\gamma_2' = \frac{g^2 - 1}{4[1 - g^2(1 - |\mu_0|)]}. \quad \text{(A6)}$$

This work was supported in part by the National Aeronautics and Space Administration under Grant NAGW-2082, Contracts NAS5-30917 and NAS5-31369, and the U.S. National Science Foundation under Grant INT-9014263. The authors are grateful to Dr. X. Li for carefully reviewing the mathematical portion of the manuscript.

REFERENCES

Abuelgasim, A. A., and Strahler, A. H. (1994), Modeling bidirectional radiance measurements collected by the Advanced Solid-state Array Spectroradiometer over Oregon transect conifer forests, *Remote Sens. Environ.* 47:261–275.

Brent, R. P. (1973), *Algorithms for Minimizing without Derivatives*, Prentice-Hall, Englewood Cliffs, NJ.

Deering, D. W. (1988), Parabola directional field radiometer for aiding in space sensor data interpretations, *Proc. SPIE* 924:249–261.

Deering, D. W, and Leone, P. (1986), A sphere-scanning radiometer for rapid directional measurements of sky and ground radiance, *Remote Sens. Environ.* 19:1–24.

Diner, D. J., Bruegge, C. J., Martonchik, J. V., et al. (1989), MISR: a multiangle imaging spectroradiometer for geophysical and climatological research for EOS, *IEEE Trans. Geosci. Remote Sens.* 27:200–214.

Gerstl, S. A. W. (1990), Physical concepts of optical and radar reflectance signatures: A summary review, *Int. J. Remote Sens.* 11:1109–1117.

Gerstl, S. A. W., and Zardecki, A. A. (1985), Coupled atmosphere / canopy model for remote sensing of plant reflectance features, *Appl. Opt.* 24:94–103.

Goel, N. S. (1988), Models of vegetation canopy reflectance and their use in estimation of biophysical parameters from reflectance data, *Remote Sens. Rev.* 4:1–222.

Goel, N. S., and Reynolds, N. (1989), Bidirectional canopy reflectance and its relationship to vegetation characteristics, *Int. J. Remote Sens.* 10:107–132.

Guzzi, R., Rizzi, R., and Zibordi, G. (1987). Atmospheric correction of data measured by a flying platform over the sea: elements of a model and its experimental validation, *Appl. Opt.* 26:3043–3051.

Hapke, B. W. (1963), A theoretical photometric function for the lunar surface, *J. Geophys. Res.* 68:4545–4570.

Hapke, B. (1986), Bidirectional reflectance spectroscopy IV: The extinction coefficient and the opposition effect, *Icarus* 67:264–280.

Iqbal, M. (1983), *An Introduction to Solar Radiation*, Academic, New York.

Irons, J. R., Ranson, K. J., Williams, D. L., Irish, R. R., and Huegel, F. G. (1991), An off-nadir pointing imaging spectroradiometer for terrestrial ecosystem studies, *IEEE Trans. Geosci. Remote Sens.* 29:66–74.

Jackson, R. D., Teillet, P. M., Slater, P. N., et al. (1990), Bidirectional measurements of surface reflectance for view angle corrections of oblique imagery, *Remote Sens. Environ.* 32:189–202.

Joseph, J. H., Wiscombe, W. J., and Weinman, J. A. (1976), The delta-Eddington approximation for radiative flux transfer, *J. Atmos. Sci.* 33:2453–2459.

Kaufman, Y. J. (1979), Effect of the Earth's atmosphere on contrast for zenith observation, *J. Geophys. Res.* 84:3165–3172.

Kieffer, H. H., Martin, T. Z., Peterfreund, A. R., and Jakosky, B. M. (1977), Thermal and albedo mapping of Mars during the Viking primary mission, *J. Geophys. Res.* 82:4249–4291.

Kimes, D. S., and Deering, D. W. (1992), Remote sensing of surface hemispherical reflectance (albedo) using portable multispectral imaging spectroradiometers, *Remote Sens. Environ.* 39:85–94.

Kimes, D. S., Newcomb, W. W., Tucker, C. J., et al. (1985), Directional reflectance factor distribution for cover types of northern Africa, *Remote Sens. Environ.* 18:1–19.

Kimes, D. S., Sellers, P. J., and Diner, D. D. (1987), Extraction of spectral hemispherical reflectance (albedo) of surfaces for nadir and directional reflectance data, *Int. J. Remote Sens.* 8:1727–1746.

Kuusk, A. (1991), Determination of vegetation canopy parameters for optical measurements, *Remote Sens. Environ.* 37: 207–218.

Lacis, A. A., and Hansen, J. E. (1974), A parameterization for the absorption of solar radiation in the earth's atmosphere, *J. Atmos. Sci.* 31:118.

Leckner, B. (1978), The spectral distribution of solar radiation at the Earth's surface—elements of a model, *Solar Energy* 20:143–150.

Lee, T., and Kaufman, Y. J. (1986), The effect of surface nonlambertian on remote sensing of surface reflectance and vegetation index, *IEEE Trans. Geosci. Remote Sens.* 24: 699–708.

Lenoble, J. (1985), *Radiative Transfer in Scattering and Absorbing Atmospheres: Standard Computational Procedures.* A Deepak Hampton, VA.

Liang, S. and Strahler, A. H. (1993a), Calculation of the angular radiance distribution for a coupled atmosphere and canopy, *IEEE Trans. Geosci. Remote Sens.* 31:491–502.

Liang, S., and Strahler, A. H. (1993b), An analytic BRDF model of canopy radiative transfer and its inversion, *IEEE Trans. Geosci. Remote Sens.* 31:1081–1092.

Liang, S., and Strahler, A. H. (1994), A four-stream solution for atmospheric radiance transfer over a non-Lambertian surface, *Appl. Opt.*, forthcoming.

Meador, W. E., and Weaver, W. R. (1980), Two-stream approximations to radiative transfer in planetary atmospheres: a unified description of existing methods and a new improvement, *J. Atmos. Sci.* 37:630–643.

Minnaert, M. (1941), The reciprocity principle in lunear photometry, *Astrophys. J.* 93:403–410.

Myneni, R. B., Ross, J., and Asrar, G. (1990), A review on the theory of photon transport in leaf canopies, *Agric. For. Meteorol.* 45:1–153.

Neckel, H., and Labs, D. (1984), The solar radiation between 3300 and 12500 A, *Solar Phys.* 90:205–258.

Penndorf, R. (1954), The vertical distribution of Mie particles in the troposphere, Geophysics Research Paper 25, AFCRL, Bedford, MA.

Peterson, D. L., and Waring, R. H. (1994), Overview of the Oregon Transect Ecosystem Research Project, *Ecol. Appl.* forthcoming.

Pinty, B., and Ramond, D. (1986), A simple bidirectional reflectance model for terrestrial surfaces, *J. Geophys. Res.* 91:7803–7808.

Powell, M. J. D. (1964), An efficient method for finding the minimum of a function of several variables without calculating derivatives, *Comput. J.* 7:155–162.

Ranson, K. J., Biehl, L. L., and Daughtry, C. S. T. (1984), *Soybean Canopy Reflectance Modeling Data Sets*, LARS Technical Report 071584, pp. 1–46.

Reitan, C. H. (1963), Surface dew point and water vapor aloft, *J. Appl. Meteorol.* 2:776.

Salomonson, V. V., and Marlatt, W. E. (1968), Anisotropic solar reflectance over white sand, snow, and stratus clouds, *J. Appl. Meteorol.* 7:475–483.

Siddall, J. N. (1972), *Analytical Decision-Making in Engineering Design*, Prentice-Hall, Englewood Cliffs, NJ.

Starks, P. J., Norman, J. M., Blad, B. L., Walter-Shea, E. A., and Walthall, C. L. (1991), Estimation of shortwave hemispherical reflectance (albedo) from bidirectional reflected radiance data, *Remote Sens. Environ.* 38:123–134.

Staylor, W. F., and Suttles, J. T. (1986), Reflection and emission models for deserts derived from Nimbus-7 ERB scanner measurements, *J. Climate Appl. Meteorol.* 25:196–202.

Tanré, D., Herman, M., Deschamps, P. Y., and de Leffe, A. (1979), Atmospheric modeling for space measurements of ground reflectances, including bidirectional properties, *Appl. Opt.* 18:3587–3594.

Tanré, D., and Legrand, M. (1991), On the satellite retrieval of Saharan dust optical thickness over land: Two different approaches, *J. Geophys. Sci.* 96:5221–5227.

Thorpe, T. E. (1977), Viking orbiter photometric observations of the Mars phase function July through November 1976, *J. Geophys. Res.* 82:4161–4165.

van de Hulst, H. C. (1980), *Multiple Light Scattering: Tables, Formulas and Applications*, Academic Press, New York.

Van Stokkom, H. T. C., and Guzzi, R. (1984), Atmospheric spectral attenuation of airborne remote sensing data: Comparison between experimental and theoretical approach, *Int. J. Remote Sens.* 5:925.

Veverka, J., and Wasserman, L. (1972). Effects of surface roughness on the photometric properties of Mars, *Icarus* 16:281–290.

Walthall, C. L., Norman, J. M., Welles, J. M., Campbell, G., and Blad, B. L. (1985), Simple equation to approximate the bidirectional reflectance from vegetation canopies and bare soil surfaces, *Appl. Opt.* 24:383–387.

Zhangwill, W. I. (1967), Minimizing a function without calculating derivatives, *Comput. J.* 10:293–296.